Hydrothermal Synthesis and characterization of brucine functionalized hydroxyapatite materials for bioimaging applications

Swadhi Radhakrishnan [1], Gayathri Krishnan [2,*], Rajesh Krishnan [3] , Anandan Kasinatha [4], Anitha Rexalin Devaraj [5]

[1] Department of Physics, Academy of Maritime Education & Training (AMET), Chennai- 603112, India; swadhi.radhakrishnan@gmail.com

[2*] Department of Physics, Academy of Maritime Education & Training (AMET), Chennai- 603112, India; gskrithick@gmail.com

[3] Department of Physics, Academy of Maritime Education & Training (AMET), Chennai- 603112, India; krishjayarajesh@gmail.com

[4] Department of Physics, Academy of Maritime Education & Training (AMET), Chennai- 603112, India; anand.nanoscience@yahoo.com

[5] Department of Physics, Academy of Maritime Education & Training (AMET), Chennai- 603112, India; anitha.rexalin@gmail.com

* Corresponding author: Gayathri Krishnan

* Corresponding author email: gskrithick@gmail.com ;

Abstract: The synthesis of new materials with decent luminescent properties signifies a challenging but imperative contribution due to their potential applications in biomedical science. In this study we evaluate the potential combinations of nanohydroxyapatite and brucine for various biomedical applications. The main objective of this study was to revel the influence of brucine ions on the design and structure of hydroxyapatite. Different concentrations of brucine (0.5%, 1%, 2%) has been incorporated with nanohydroxyapatite. The morphology and structure, as well as the optical properties, of the obtained nanomaterials were characterized using X-ray powder diffraction analysis (XRD), Fourier Transform Infrared spectrometry (FTIR), SEM microscopy, UV-Vis spectroscopy. The measurements revealed that brucine ions were integrated into the structure of hydroxyapatite in all the composition. The biocompatibility and cytotoxicity of the obtained powders evaluated using MTT assay and fluorescent spectroscopy reveals the ability of the synthesized nanomaterials to be used for biological system imaging.

Keywords: Nanoparticles; Biomaterials; Fluorescence studies; optical studies; X-ray diffraction

1. Introduction

Multifunctional nanoparticles are of great interest for new applications such as cellular imaging, drug delivery and tumor therapy. An increasing number of surface chemistry strategies have been used to transform these nanosystems through surface modifications such as establishing polymer surface coatings and surface grafting with small

molecules. Among them, small-molecule surface modification is one of the most widely used methods, with advantages such as rapid and gentle manufacturing process, good biocompatibility and dominating fluorescence properties. In recent years, efforts have been made to develop nanocrystalline calcium phosphate to improve its biological, functional and mechanical properties for their use in biomedical applications. Calcium phosphate is the major component of bone and teeth. Calcium phosphate was classified into different types based on their stoichiometry Ca/Po ratio. The Stoichiometry Ca/Po ratio as 1:67 is known as hydroxyapatite (HAP) with the chemical formula (Ca10(Po4)6 (OH)2) [1-5]. HAP is a synthetic ceramic biomaterial which is considered to be the most firm (Calcium Phosphate) biomaterial in the biological environment [6-8]. HAP shows exceptional biocompatibility, non-toxic, non-immunogenic, bioactive and high osteoinductive [9,10]. HAP can directly bond with the human tissues and it has high constancy and flexibility [10]. First HAP was proposed for the hard tissue engineering applications. Then the current study initiates that, HAP nanoparticles offers good opportunity especially in cancer therapy among other biomaterials [6,11]. HAP is used for biomedical application such as drug delivery, dental implants, augmentation, orthopedics [12-19].

The biological response of HAP depends on their physicochemical properties such as particle size, degree of crystallinity, surface area, morphology and surface charge. HAP with various properties and solubility could improve the bone formation, prevents the growth of cells and tissues. The cancer treatment includes chemotherapy, radiotherapy and surgery. Chemotherapy lags with the toxicity towards the normal cell and for this reason, drug delivery seeks the attention for the active targeting of cancer cells with an anticancer drug [6].

HAP can synthesis by numerous methods such as precipitation method [9,20], Sol-gel [20-23], hydrothermal, Solid state reaction, RF plasma spray, mechano chemical, micro emulsion[12,20]. Hydrothermal method was frequently used to obtain good morphology of nanosized materials [23-27].

The anticancer agent which is used was about 60% of natural medicine. Natural drug offers safe, cost-effective and diverse biological- medical activities. Only few natural drugs are in clinical purpose because of their limitations such as poor water stability, low bioavailability, short half-life and non-specific targeting. Nano sized medicine has the potential to solve these limitations [28-31].

Modern research shows the alkaloid as a main active ingredient for the content of about 5% of crude drugs, particularly brucine, strychnine and its nitrogen oxide, of which brucine grabs 1%. Brucine is a natural, weakly basic indole alkaloid from mature seeds of Strychnos nux-vomica Linn. from East India, Burma, Thailand, China and Australia [32]. It has been used as a traditional Chinese medicine for treating various disease such as diabetes, anaemia, gonorrhoea, liver cancer. It helps to improve the blood circulation and rheumatic pain relief [33]. Brucine with the molecular formula of (C23H26N2O4), which is white crystalline powder, tastes bitter, slightly soluble in water and its soluble in ether, chloroform, ethanol, methanol and other organic solvents. Brucine is a good analgesic, anti-inflammatory, anti-tumor. Brucine is mainly engrossed for reducing the toxicity by transdermal administration and refining the efficiency through a novel drug carrier. As brucine has

exceptional antitumor activity, it plays an effective therapeutic agent for colon cancer for decreasing the tumour weight and volume [28, 32]. The objective of the work is to synthesis the Brucinium hydroxyapatite (BHAP) nanoparticles for theranostic and bio imaging applications.

2. Materials and Methods

2.1. Synthesis of BHAP

Brucine (C23H26N2O4) (Loba- 99%), calcium nitrate tetrahydrate (Ca(NO3)2.4H2O) (Merck >98.0%) ,0.6M di-ammonium hydrogen phosphate ((NH4)2 HPO4 (Sisco >99%)and Liquid ammonia for pH adjustment.

BHAP nanoparticles was synthesized by hydrothermal method. The dopant (Br- 0.5%, 1%, 2%) were added to the calcium solution then mixed with the phosphate solution to obtain brucine hydroxyapatite (BHAP) with various concentrations. pH was adjusted to 9 by adding liquid ammonia, then the solution was kept at 180°C for 24hrs. Then it was centrifuged and dried at 100°C.

2.2. Characterization Methods

The X-ray powder diffraction (XRD) measurements were done using a BRUKER USA D8 Advance, Davinci X-ray diffractometer with Cu Kα ((k = 1.540 Å) to determine the phase and structure of the particles. The morphology of the BHAP nanoparticles was characterized by using a Scanning electron microscope (SEM) using CAREL ZEISS, Model: EVO 18. Dynamic Light Scattering (DLS) measurements were done using a Micromeritics Model: Nano Plus with a 70 mW diode laser (660 nm). All data were obtained at 160° and 15° measurement angles and averaged over 12 scans. The vibrational analysis of the synthesized BHAP was done by using FTIR spectra. The FTIR spectrum was recorded by Perkin Elmer spectrum Two Fourier Transform infrared spectrometer in the wavenumber range 400 - 4000 cm-1. The assignment of bands observed in the vibration spectra is essential step for solving structural and chemical problems. The UV–vis–NIR optical absorption spectrum was collected using a spectrophotometer (Perkin Elmer Lambda 950, U.S.). Fluorescence characterization of the synthesized particles were done by exciting the sample with a 300 nm power tunable 14-Pin butterfly module laser diode (Perkin Elmer Model: LS 45 Range: 200nm to 900nm) that was controlled by a laser diode driver (Thorlabs LM74S2 Driver, Thorlabs Laser Diode Control LDC2000-2A). Fluorescence characterization of the synthesized nanocrystals was done using a Perkin Elmer Model: LS 45 in the Range of 200 to 900 nm. The cytotoxicity of BHAP was tested using dose dependent MTT assays in Mice fibroblast cell to study the toxicity and biocompatibility of the synthesized material.

3. Results and Discussion

3.1. X-ray diffraction analysis

The XRD patterns (Figure.1) of pure HAP and HAP synthesized using 0.5%, 1% and 2% of brucine show evidence of diffraction peaks of the standard hydroxyapatite (JCPDS No.9-0432) [34]. The main phase in all samples was identified as hydroxyapatite (JCDPS No.01-074-0566). HAP showing space group P63 /m with a hexagonal structure. It can be seen that, the lattice parameters of the prepared samples are in excellent agreement with standard data a=b=9.4240 Å, c=6.8790 Å. The broad peak observed in the region 30–40° can be predicted to (211), (112), (300) and (202) reflections of HAP. The results of XRD pattern elucidate that the crystalline size slightly increased with increasing the concentration of brucine. The changes in the size, shape and dimension of the nanorods are perceived when 2% of brucine was used. The increases in the width of a particular peak indicate the changes in respective crystal phase. The XRD pattern shows that some changes happened in the crystal plane by the addition of brucine. Gaussian fit was used to calculate the full width at half maxima for the determination of crystallite size (D) by using Scherrer equation:

$$D = \frac{0.9\lambda}{\beta\ Cos\theta}$$

Where, D is the crystallite size, λ is the wavelength of Cu-Kα radiations (λ=1.5405 Å), θ is the corresponding Braggs diffraction angle and β is full width at half maxima of the peaks. The average crystallite sizes of HAP and BHAP were found to be around 82 nm to 90 nm, respectively. About pure HAP similar result and phase purity were observed in our previous researcher [35]. The reflection peaks are quite broad, signifying their Nano-crystallinity.

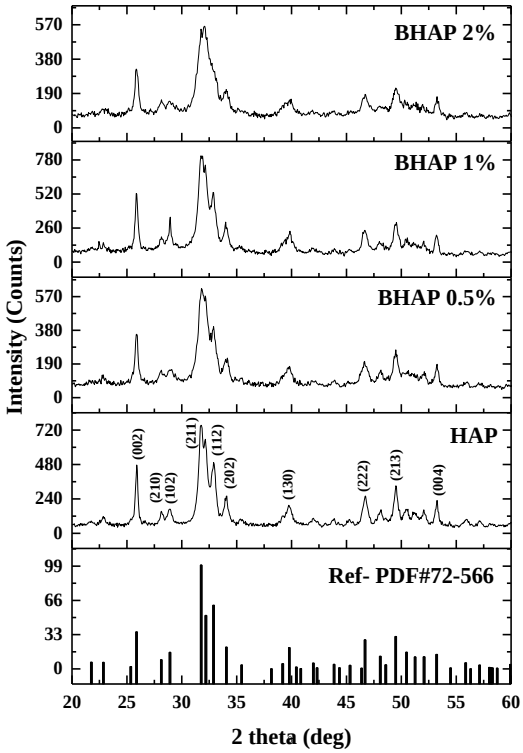

Figure 1. XRD pattern of BHAP particles in comparison with standard reference

3.2. Analysis of Particle Size Distribution by DLS Technique

Dynamic light scattering (DLS) is a recognized measurement technique for the characterization of particle sizes in suspension, based on the Brownian motion of particles. The smaller the particles, the faster they will move in a solution. The hydrodynamic diameter indicates the particle size plus the dielectric layer, which adheres to its surface during movement through the liquid medium. The movement of the particles causes intensity variations in the scattered light. From these fluctuations, the diffusion coefficient can be resolute, and thus the hydrodynamic diameter of the particle is attained from the Stokes–Einstein equation:

$$d(H) = \frac{kT}{3\pi\eta D}$$

where: d(H) = hydrodynamic diameter, k = Boltzmann's constant (1.38 × 10−23 NmK−1), T = absolute temperature (K), η = solvent viscosity (N·s·m−2), and D = diffusion coefficient (m2·s−1). The DLS measurement of the BHAP is shown in Figure.2. The average particle size (hydrodynamic diameter in aqueous solutions) varies between 76 nm and 97 nm, with a monomodal size distribution. The low values of the polydispersity index suggest that the investigated samples are homogenous in size. The PdI is situated in the range of 0.009–0.087.

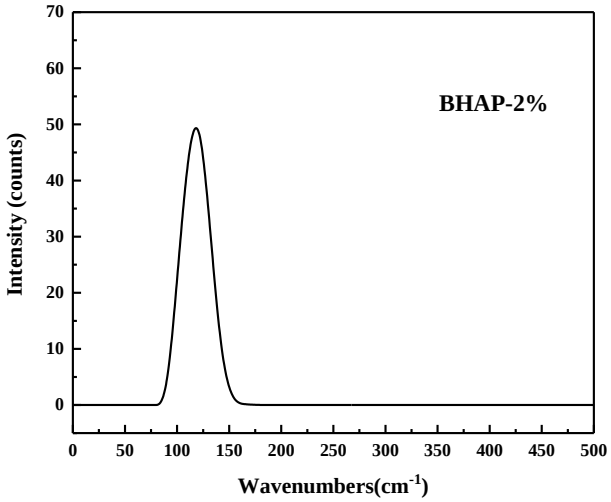

Figure 2. Dynamic Light Scattering (DLS) measurement of BHAP(2%) nanoparticles.

3.3. Scanning Electron Microscope

SEM was used to study about the morphology of nanoparticles. Figure.3a & 3b shows the morphology of hydroxyapatite and brucinium hydroxyapatite. The morphology was found to be highly agglomerated; this happens due the Oswarld's ripping [36]. By incorporating brucine ions with hydroxyapatite, the morphology was modified. Thus, the nanoparticles become spherical, the agglomerates denser. The shape of the hydroxyapatite was observed as rod shape, whereas brucinium hydroxyapatite as a clamped spherical shape. The size of the brucinium HAP is about 70nm to 120nm.

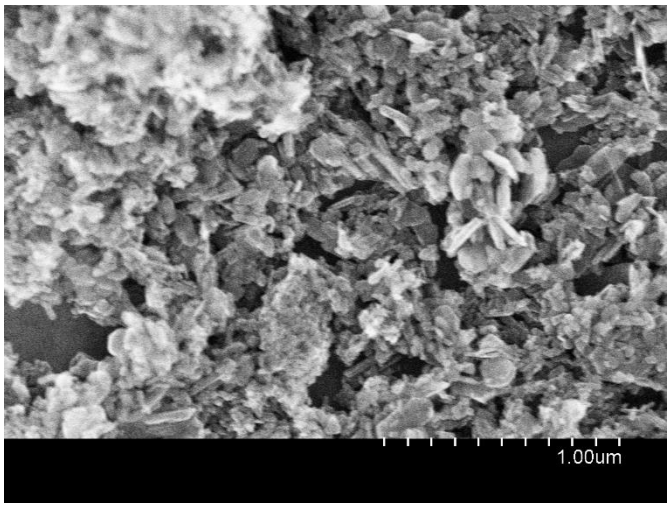

Figure 3(a). SEM micrograph of HAP nanoparticles.

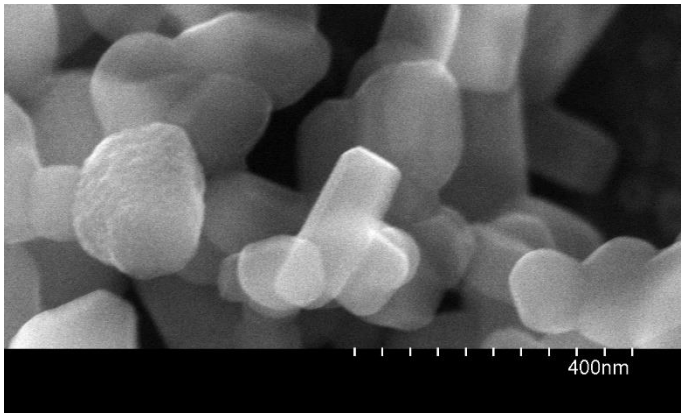

Figure 3(b). SEM micrograph of BHAP (2%) nanoparticles

3.4. FT- IR spectral analysis

The FTIR spectrum of synthesized HAP and BHAP is shown in the Figure.4. The characterized peak shown at 551cm^{-1}, 605cm^{-1} corresponds to Asymmetric bending vibration of P-O and 632cm-1, 2393cm-1 corresponds to O-H vibration. The prominent peak at 1032 cm^{-1} is due to the asymmetric bending of P-O bond of phosphate group. The peak at 1392 cm^{-1} and 1712 cm^{-1} describes the C=C stretch and the aromatic stretch of C=O bending due to H2O molecules [37]. The peaks at 826 cm^{-1}, 1385cm^{-1}, 1637 cm^{-1}, 3130 cm^{-1} shows prominent effect of brucine with hydroxyapatite [37,38]. The Strong peak shown at 1381 cm^{-1} evident the hydrogen formation of the brucine [38]. The absorption at 3130 cm^{-1} and 1381 cm^{-1} plays the role of BHAP due to stretching of N-H and N-O bonding. The peak at the IR region of 2393 cm^{-1} of brucine supports the hydrogen bonding [38]. Thus, peak at 2393 cm^{-1} contribute to the hydrogen bonding of brucine. The other observed IR bands with their tentative assignments of various functional groups are presented in Table. 1.

IR Peak (cm^{-1})	Assignment	IR Peak (cm^{-1})	Assignment
551, 605	P-O, Asymmetric bending vibration	1637	C=C, stretch
632,2393	O-H, Vibration	1712	C=O, stretch
826	=C-H, bending	3130	N-H, stretch
1032, 1381	C-O, stretch	3416, 3580	O-H, stretch

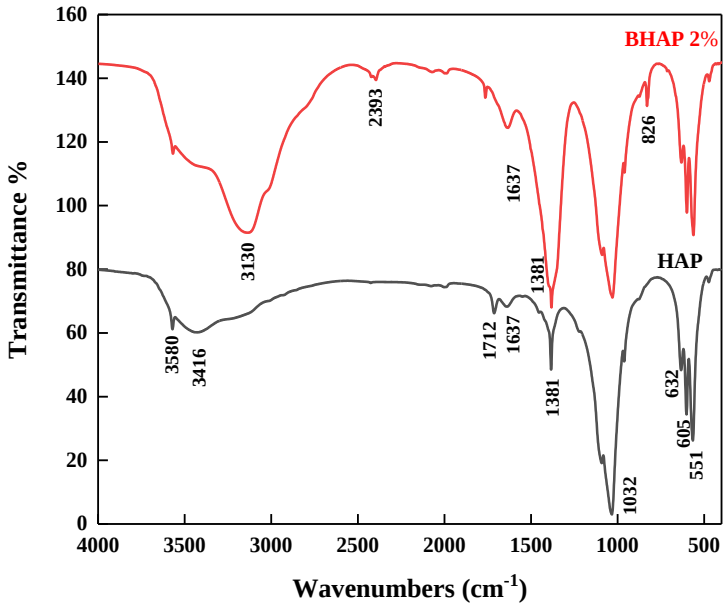

Figure 4. IR vibrational spectrum of HAP and BHAP (2%) nanoparticles

Table 1. FTIR peak assignment of HAP and BHAP (2%) nanoparticles

3.5. ICP-OES Analysis

Element analysis was done using the ICP-OES (Inductively Coupled Plasma—Optical Emission Spectrometers, Agilent 720 apparatus,) technique (Table.2) in order to confirm the composition and homogenous distribution of the Ca and P. All of the constituting elements were in a proper molar ratio confirming right stoichiometry of the final material. The ratio of the Ca2+ cation to the P5+ was about 1.67 for all samples, well matching with the theoretical ratio of Ca/P in calcium hydroxyapatite.

Table 2. Results of the ICP-OES analysis of the BHAP nanoparticles.

Sample Mass (g)	Sample	Ca (mg/ml)	P (mg/ml)	Ca (mol)	P (mol)	Ca/P
0.1	HAP	382.5	176.5	0.9544	0.5698	1.675
o.1	BHAP	378.8	174.8	0.9452	0.5643	1.674

3.6. UV-Vis- Spectral analysis

The optical absorption spectrum of the prepared nano powders shows the presence of an extensive transparency window lying between 300-1100 nm for the 2% BHAP sample. It was also clear that the percentage of transmittance increases with increase in brucine concentration. The obtained transmission spectrum of the pure and brucine functionalised hydroxyapatite samples is shown in Figure 5. The band gap energy was calculated using Tauc's plot and the estimated values was 5.21 eV for the 2% brucine substitute HAP. The plot of variation of $(\alpha h\nu)2$ vs. $h\nu$ (eV) is shown in Fig.6. The linear portion of the plot at the absorption edge confirms that the crystal has a direct optical band gap. The direct optical band gap of the crystal can be evaluated by the extrapolated line with the photon energy axis (at D= 0) of the linear part which is found to be 5.21 eV. As a consequence of a wide band gap, the synthesized material has a large transmittance in the visible region.

3.7. Fluorescence Spectroscopy

In common, HAP is not a fluorescent material, though, in this study all the BHAP nanoparticles synthesized by Hydrothermal method at room temperature using water/ DMSO as solvents exhibited yellow, green and red fluorescence. The mechanism of the fluorescence of the newly synthesized BHAP nanoparticles is not very clear at this stage, because neither Ca2+ nor PO4 3− or brucine is known to show any fluorescing property; hence, this comportment could be attributed to self-propelling fluorescence of these particles. Previously, limited researchers have reported the synthesis of self-activated fluorescence in HAP wherein fluorescence has been accredited to the existence of the CO•• radical in the crystal lattice, introduced through the precursor materials [39-43]. All of these studies have shown blue emission with maxima between 400 and 460 nm. In the present work, all BHAP prepared by the hydrothermal method exhibit a small emission at 750 nm to 820 nm around the red region (shown as inset in Fig.7). This may be attributed to the combination of brucine and hydroxyapatite ions. This observation further underlines the reputation of asymmetry for optical activity. Further experiments are underway to explicate the complete mechanism of fluorescence in BHAP and will be reported elsewhere.

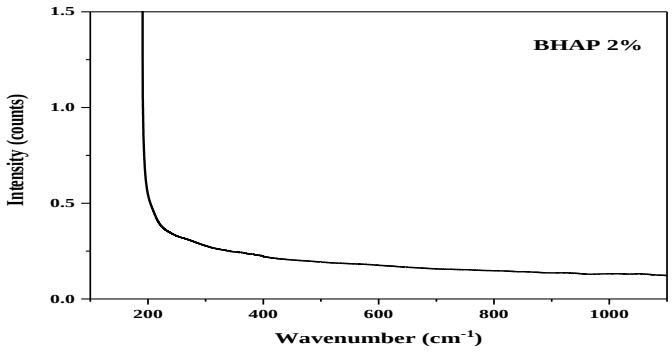

Figure 5. Optical absorption spectrum of BHAP (2%) nanoparticles

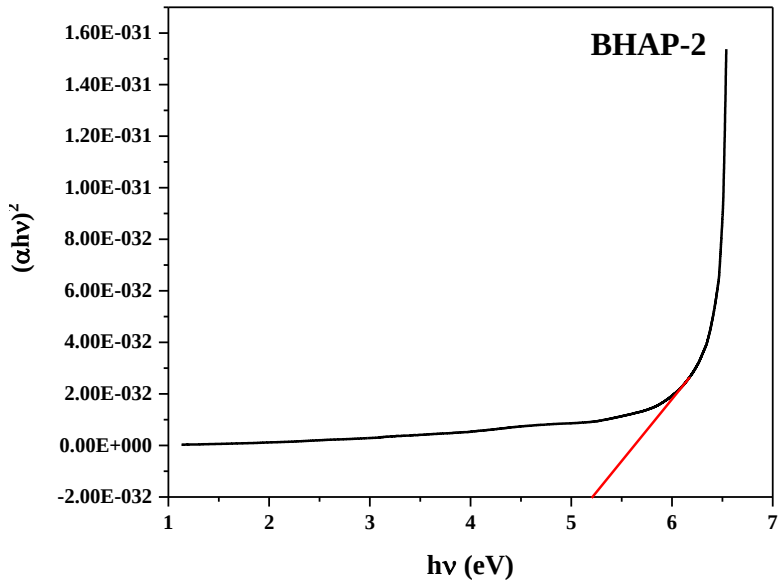

Figure 6. Bandgap measurement using Tauc's plot for BHAP (2%) nanoparticles

3.8. Cytotoxicity-MTT Assay

Cytotoxicity was measured by the MTT (3-(4,5-dimethylthiazol-2-yl)-2,5-diphenyltetrazolium bromide) method [44]. Exponentially growing mice cells werze inoculated with 5 × 104 cells/well supplemented with complete media. The cells were exposed to various concentrations (25, 50,100, and 200 µg/ mL) of the BHAP dispersed in DMEM, and incubated for 24 h. MTT (20 µL of 5 mg/mL) was added to the test samples, and the plates were incubated at 37 °C for 4 h. The medium was pipetted out carefully without disturbing the cells after 4 h. For dissolving the formazan crystals, 150 µL of DMSO was added, and the absorbance was measured at 570 nm using a UV−vis spectrophotometeter (UV2450). All measurements were done in triplicate. The relative cell viability (%) was calculated as

$$\frac{A_t}{A_c} \times 100$$

[At] is the absorbance of the test sample, and [Ac] is the absorbance of the cells without treatment. Biolabeling and bioimaging are imperative techniques for detection and diagnosis of diseases. To use any material for such purposes, its cytotoxicity/biocompatibility needs to be calculated. In recent era, use of lanthanide doped HAP and other plant-based materials incorporated HAP nanoparticles has successfully resulted in a series of multifunctional materials for bioimaging and biolabeling [45, 46]. However, rare earth

elements are toxic and have adverse effects due to their accumulation in the body [46]. Many of the plant extracts also doesn't show a considerable compatibility. The compatible nature of the brucine and their applications in the theranostic field has been already reported [19,31]. In the current study, we have synthesized a new-fangled BHAP with self-activated fluorescence properties. Since these BHAP do not contain any toxic dopants, they may be used as safe alternatives for bioimaging. The cytotoxicity of BHAP was tested using dose dependent MTT assays in Mice fibroblast cell. MTT assay is mainly based on enzymatic reduction of MTT dye. After 24 hours, an MTT assay was used to assess the toxicity of nanoparticles at these concentrations. From the Figure.8, for the BHAP nanoparticle concentrations, the cell viability was above 80% which shows that the synthesized particles do not exhibit high toxicity and are biocompatible for use in bioimaging applications.

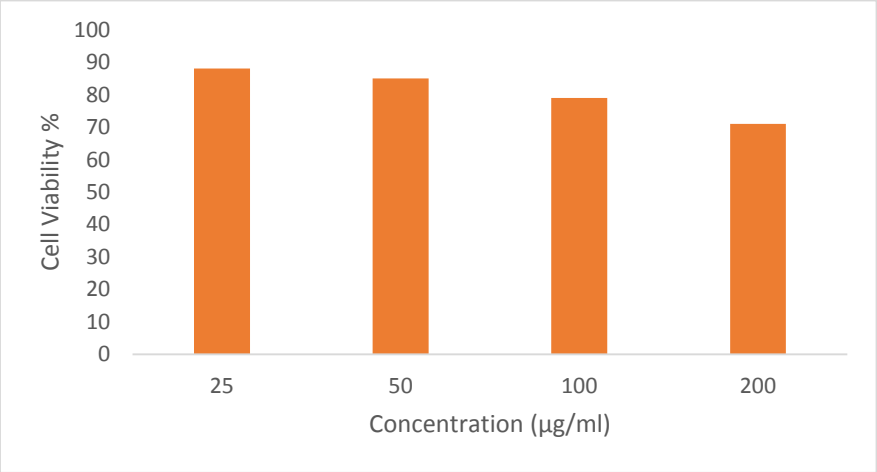

Figure 8. Invitro toxicity study of BHAP nanoparticles

4. Conclusions

A new class of Brucine functionalized hydroxyapatite nanoparticles was synthesized through hydrothermal method. In the present study, we attempted to understand the various properties BHAP nanoparticles. The effects of brucine on HAP were examined through morphology, UV absorption, and fluorescence spectroscopy. The XRD and FTIR studies confirm the structure of the synthesized nanoparticle. The results of our MTT assay show no significant cellular toxicity for concentrations up to 200 µg ml-1. Considering the improved biocompatibility of HAP, the present BHAP could offer plentiful exciting applications in the field of biomedical area such as bio-imaging, targeted drug delivery and other image guided therapeutic application.

Funding

"This research received no external funding"

Conflicts of Interest

"The authors declare no conflict of interest."

References

1. Jae-Kil Han, Ho-Yeon Song, Fumio Saito, Byong-Taek Lee, Synthesis of high purity nano-sized hydroxyapatite powder by microwave-hydrothermal method, Materials Chemistry and Physics, 99 (2006) 235–239. https://doi.org/10.1016/j.matchemphys.2005.10.017
2. Peipei Wang, Caihong Li, Haiyan Gong, Xuerong Jiang, Hongqiang Wang, Kaixing Li, Effects of synthesis conditions on the morphology of hydroxyapatite nanoparticles produced by wet chemical process, Powder Technology, 203 (2010) 315–321. https://doi.org/10.1016/j.powtec.2010.05.023 .
3. Oliveira, É. R.; Nie, L.; Podstawczyk, D.; Allahbakhsh, A.; Ratnayake, J.; Brasil, D. L.; Shavandi, A. Advances in Growth Factor Delivery for Bone Tissue Engineering. Int. J. Mol. Sci. 2021, 22, 903-935, https://doi.org/10.3390/ijms22020903 .
4. Lett, J. A; Sagadevan, S.; Fatimah, I.; Hoque, M. E.; Lokanathan, Y.; Léonard, E.; Alshahateet, S. F.; Schirhagl, R.; Oh, W. C. Recent advances in natural polymer-based hydroxyapatite scaffolds: properties and applications. Eur. Polym. J. 2021, 148, 110360, https://doi.org/10.1016/j.eurpolymj.2021.110360 .
5. Montoya, C.; Du, Y.; Gianforcaro, A. L.; Orrego, S.; Yang, M.; Lelkes, P. I. On the road to smart biomaterials for bone research: definitions, concepts, advances, and outlook. Bone Res. 2021, 9, 1-16, https://doi.org/10.1038/s41413-020-00131-z .
6. Kargozar, S.Mollazadeh, S. Kermani, F.Webster, T.J. Nazarnezhad, S. Hamzehlou, S. Baino, F, Hydroxyapatite Nanoparticles for Improved Cancer Theranostics. J. Funct. Biomater, 13 (2022) 100. https://doi.org/10.3390/jfb13030100 .
7. S, S.; S, R.; L, K.; Dhanaraj, G. Novel and naturally derived Hydroxyapatite/cellulose nanofibre/curcumin biocomposite for tissue engineering applications. Res.Sq 2021, 1, 1–20, https://doi.org/10.21203/rs.3.rs332070/v1 .
8. 7. Nathanael, A. J.; Oh, T. H. Encapsulation of calcium phosphates on electrospun nanofibers for tissue engineering applications.Crystals 2021, 11, 199–221, https://doi.org/10.3390/cryst11020199 .
9. I. Mobasherpour, M. Soulati Heshajin, A. Kazemzadeh, M. Zakeri, Synthesis of nanocrystalline hydroxyapatite by using precipitation method, Journal of Alloys and Compounds 430 (2007) 330–333. https://doi.org/10.1016/j.jallcom.2006.05.018 .
10. Marcelo F. Cipreste, Anderson M. Peres, Alexandre A.C. Cotta, Fermin H. Arag_on, Alan de M. Antunes, Alexandre S. Leal, Waldemar A.A. Macedo, Ed_esia M.B. de Sousa, Synthesis and characterization of 159Gd-doped hydroxyapatite nanorods for bioapplications as theranostic systems, Materials Chemistry and Physics, (2016), https://doi.org/10.1016/j.matchemphys.2016.06.063 .
11. Luo, D. Xu, X. Iqbal, M.Z. Zhao, Q. Zhao, R. Farheen, J. Zhang, Q. Zhang, P. Kong, X., siRNA-Loaded Hydroxyapatite Nanoparticles for KRAS Gene Silencing in Anti-Pancreatic Cancer Therapy, Pharmaceutics, 13 (2021), 1428. https://doi.org/10.3390/pharmaceutics13091428 .
12. Li-yun Cao, Chuan-bo Zhang, Jian-feng Huang, Synthesis of hydroxyapatite nanoparticles in ultrasonic precipitation, Ceramics International, 31 (2005), 1041–1044. https://doi.org/10.1016/j.ceramint.2004.11.002
13. Errich, A; Azzaoui, K.; Mejdoubi, E.; Hammouti, B.; Abidi, N.; Akartasse, N.; Benidire, L.; Hajjaji, S. El.; Sabbahi, R.; Lamhamdi, A. Toxic heavy metals removal using a hydroxyapatite and hydroxyethyl cellulose modified with a new gum Arabic. Indones. J. Sci. Technol. 2021, 6, 41–64, https://doi.org/10.17509/ijost.v6i1.31480 .
14. Bhandari, N.L.; Bista, S.; Gautam, T.R.; Bist, K.; Bhandari, G.; Subedi, S.; Dhakal, K.N.. An overview of synthesis based biomedical applications of Hydroxyapatite Nanomaterials. J. Nepal Chem. Soc. 2021, 42, 64- 74, https://doi.org/10.3126/jncs.v42i1.35333 .

15. Pandey, G.; Dhaka, K. N.; Singh, A. K.; Dhungel, S. K.; Adhikari, R. Facile methods of preparing pure hydroxyapatite nanoparticles in ordinary laboratories. Bibechana. 2021, 18, 83–90, https://doi.org/10.3126/bibechana.v18i1.29600 .
16. Chen, D.; Zhao, J.; Jiang, X. Synthesis and characterization of silver substituted strontium phosphate silicate apatite using solid-state reaction for osteoregenerative applications. Bioengineered. 2021, 12, 1111–1125, https://doi.org/10.1080/21655979.2021.1899670 .
17. Sočo, E.; Papciak, D.; Michel, M.M.; Pająk, D.; Domoń, A.; Kupiec, B. Characterization of the physical, chemical, and adsorption properties of coal-fly-ash–hydroxyapatite composites. Minerals 2021, 11, 774-792, https://doi.org/10.3390/min11070774 .
18. Cestari, F.; Agostinacchio, F.; Galotta, A.; Chemello, G.; Motta, A.; M. Sglavo, V. Nano-hydroxyapatite derived from biogenic and bioinspired calcium carbonates: synthesis and in vitro bioactivity. Nanomaterials 2021, 11, 264-277, https://doi.org/10.3390/nano11020264 .
19. LI Miao, LI Ping, ZHANG Mei, and MA Feng, Brucine suppresses breast cancer metastasis via inhibiting epithelial mesenchymal transition and matrix metalloproteinases expressions Chinese Journal of Integrative Medicine, 24[1] (2017), 40-46, https://doi.org/10.1007/s11655-017-2805-1 .
20. Burcu Cengiz, Yavuz Gokce, Nuray Yildiz, Zeki Aktas, Ayla Calimli, Synthesis and characterization of hydroxyapatite nanoparticles, Colloids and Surfaces A: Physicochem. Eng. Aspects, 322 (2008), 29–33. https://doi.org/10.1016/j.colsurfa.2008.02.011 .
21. Il-Seok Kim, Prashant N. Kumta, Sol–gel synthesis and characterization of nanostructured hydroxyapatite powder Materials Science and Engineering B, 111 (2004), 232–236. https://doi.org/10.1016/j.mseb.2004.04.011 .
22. Yingjun Wang, Shuhua Zhang , Kun Wei, Naru Zhao, Jingdi Chen, Xudong Wang, Hydrothermal synthesis of hydroxyapatite nanopowders using cationic surfactant as a template Materials Letters, 60 (2006), 1484–1487. https://doi.org/10.1016/j.matlet.2005.11.053 .
23. J S Earl, D J Wood and S J Milne, Hydrothermal synthesis of hydroxyapatite, Journal of Physics: Conference Series, 26 (2006), 268–271, https://iopscience.iop.org/article/10.1088/1742-6596/26/1/064/pdf .
24. S. Senthilkumar, V. Dhivya, M. Sathya & A. Rajendran RETRACTED ARTICLE: Synthesis and characterization of magnetite/hydroxyapatite nanoparticles for biomedical applications, Journal of Experimental Nanoscience, 2021,16:1, 159-179, https://doi.org/10.1080/17458080.2021.1931685
25. Kermani, F.; Mollazadeh, S.; Kargozar, S.; Vahdati Khakhi, J. Improved osteogenesis and angiogenesis of theranostic ions doped calcium phosphates (CaPs) by a simple surface treatment process: A state-of-the-art study. Mater. Sci. Eng. C 2021, 124, 112082, https://doi.org/10.1016/j.msec.2021.112082 .
26. Lara-Ochoa, S.; Ortega-Lara, W.; Guerrero-Beltran, C.E. Hydroxyapatite Nanoparticles in Drug Delivery: Physicochemistry and Applications. Pharmaceutics 2021, 13, 1642, https://doi.org/10.3390/pharmaceutics13101642
27. Nongshan Zhang, Yiyun Wu, Runlin Xing, Bo Xu, Dai Guoliang, and Peimin Wang, Effect of Ultrasound-Enhanced Transdermal Drug Delivery Efficiency of Nanoparticles and Brucine, BioMed Research International Volume 2017, Article ID 3273816. https://doi.org/10.1155/2017/3273816 .
28. Khaled AbouAitah, Agata Stefanek, Iman M. Higazy, Magdalena Janczewska, Anna Swiderska-Sroda, Agnieszka Chodara, Jacek Wojnarowicz, Urszula Szałaj, Samar A. Shahein, Ahmed M. Aboul-Enein, Faten Abou-Elella, Stanislaw Gierlotka, Tomasz Ciach and Witold Lojkowski, Effective Targeting of Colon Cancer Cells with Piperine Natural Anticancer Prodrug Using Functionalized Clusters of Hydroxyapatite Nanoparticles, Pharmaceutics,12 (2020), 70. https://doi.org/10.3390/pharmaceutics12010070 .
29. Jianmin Qin, Lin Yang, Xia Sheng, Zhongqiu Sa, Tao Huang, Qi Li, Kepan Gao, Qinghua Chen, Jingwei Ma And Hebai Shen, Antitumor effects of brucine immuno-nanoparticles on hepatocellular carcinoma in vivo, Oncology Letters 15, (2018), 6137-6146,. https://doi.org/10.3892/ol.2018.8168 .
30. Hu Ke-Fei1, Kong Xiang-Ying2, Zhong Mi-Cun2, Wan Hong-Ye2, Lin Na2, And Pei Xiao-Hua3, Brucine inhibits bone metastasis of breast cancer cells by suppressing Jagged1/Notch1 signaling pathways, Chinese Journal of Integrative Medicine, Feb 23[2] (2017), 110-116. https://doi.org/10.1007/s11655-016-2647-2 .

31. Guangwen Shu, Xue Mi, Jian Cai, Xinlin Zhang, Wu Yin, Xinzhou Yang, You Li, Lvyi Chen, Xukun Deng, Brucine, an alkaloid from seeds of Strychnos nux-vomica Linn., represses hepatocellular carcinoma cell migration and metastasis: The role of hypoxia inducible factor 1 pathway , Toxicology Letters, 222 (2013), 91–101. https://doi.org/10.1016/j.toxlet.2013.07.024 .
32. Khelendra Agrawal, Gurbhinder Singh, Devendra Puri, Satya Prakash, Synthesis and Characterization of Hydroxyapatite Powder by Sol-Gel Method for Biomedical Application Journal of Minerals & Materials Characterization & Engineering, Vol. 10 [8] (2011), 727-734, http://dx.doi.org/10.4236/jmmce.2011.108057
33. Suresh Kumar, G., Govindan, R., Girija, E.K., In situ synthesis, characterization and in vitro studies of ciprofloxacin loaded hydroxyapatite nanoparticles for the treatment of osteomyelitis, J. Mater. Chem. B. 2, (2014), 5052–5060. https://doi.org/10.1039/C4TB00339J .
34. Sneha S Bandgar, Tanaji V Kolekar, Shailesh S Shirguppikar, Mahesh A Shinde, Rajendra V Shejawal, Sambhaji R Bamane, Synthesis, Characterization of Silver Doped Hydroxyapatite Nanoparticles for Biomedical Applications, Der Pharma Chemica, 9[3] (2017), 78-84 https://www.derpharmachemica.com/author/sneha-s-bandgar-2255 .
35. Arunseshan Chandrasekar, Suresh Sagadevan and Arivuoli Dakshnamoorthy, Synthesis and characterization of nano-hydroxyapatite (n-HAP) using the wet chemical technique, International Journal of Physical Sciences, Vol. 8(32), (2013) pp. 1639-1645, https://doi.org/10.5897/IJPS2013.3990 .
36. Ammar Z. Alshemary, Muhammed Akram, Yi-Fan Goh, Mohammed Rafiq, Abdul Kadir, Ahmad Abdolahi, Rafaqat Hussain, Structural characterization, optical properties and in vitro bioactivity of mesoporous erbium-doped hydroxyapatite, Journal of Alloys and Compounds, 645 (2015), 478-486. https://doi.org/10.1016/j.jallcom.2015.05.064 .
37. Aboothahir Afzal, Mohamed Shahin Thayyil, Mohammad Shariq, Yohannan Sheena Mary, Kaippallil Sundaresan Resmi, Renjith Thomas, Nasarul Islam, and Ajithan Jyothi Abinu, Anti-Cancerous Brucine and Colchicine: Experimental and Theoretical Characterization, ChemistrySelect, 4, (2019), 11441– 11454. https://doi.org/10.1002/slct.201902698 .
38. Zhang, C.; Yang, J.; Quan, Z.; Yang, P.; Li, C.; Hou, Z.; Lin, Hydroxyapatite Nano- and Microcrystals with Multiform Morphologies: Controllable Synthesis and Luminescence Properties, J. Cryst. Growth Des.9[6] (2009), 2725−2733. https://doi.org/10.1021/cg801353n .
39. Zhang, C.; Li, C.; Huang, S.; Hou, Z.; Cheng, Z.; Yang, P.; Peng, C.; Lin, Self-activated luminescent and mesoporous strontium hydroxyapatite nanorods for drug delivery, J, Biomaterials, 31[12] (2010), 3374−3383. https://doi.org/10.1016/j.biomaterials.2010.01.044 .
40. Ning, Z.; Chang, Z.; Li, W.; Sun, C.; Zhang, J.; Liu, Y. Solvothermal synthesis and optical performance of one-dimensional strontium hydroxyapatite nanorod. Chin. J. Chem. Eng 20[1], (2012), 89−94 https://cjche.cip.com.cn/EN/Y2012/V20/I1/89 .
41. Kumar, G. S.; Girija, E.; Thamizhavel, A. Synthesis and photoluminescence study of flower-like hydroxyapatite nanostructure for bioprobe applications. AIP Conf. Proc. (2012),57.250. https://doi.org/10.1063/1.4791005 .
42. Zhang, C.; Lin, Defect-related luminescent materials: synthesis, emission properties and applications, J. Chem. Soc. Rev, 41 [23] (2012), 7938−7961. https://doi.org/10.1039/C2CS35215J .
43. T. Mossman, Rapid colorimetric assay for cellular growth and survival: Application to proliferation and cytotoxicity assays ,J. Immunol. Methods, 65 (1983), 55–63. https://doi.org/10.1016/0022-1759(83)90303-4.
44. Resch-Genger, U.; Grabolle, M.; Cavaliere-Jaricot, S.; Nitschke, R.; Nann,T, Quantum dots versus organic dyes as fluorescent labels, Nat. Methods, 5 [9] (2008), 763−775. https://doi.org/10.1038/nmeth.1248 .
45. Mondejar, S. P.; Kovtun, A.; Epple, M, Lanthanide-doped calcium phosphate nanoparticles with high internal crystallinity and with a shell of DNA as fluorescent probes in cell experiments, J. Mater. Chem, 17 [19] (2007), 4153−4159. https://doi.org/10.1039/B708258D .
46. Ge, K.; Zhang, C.; Jia, G.; Ren, H.; Wang, J.; Tan, A.; Liang, X. J.; Zang, A.; Zhang, Defect-Related Luminescent Mesoporous Silica Nanoparticles Employed for Novel Detectable Nanocarrier, J. ACS Appl. Mater. Interfaces 7 [20] (2015), 10905−14 https://doi.org/10.1021/acsami.5b02146